

DESTABILISING EFFECTS OF PLANT FLEXIBILITY IN AIR AND AQUATIC VEGETATION CANOPY FLOWS

F. Gosselin & E. de Langre

Département de Mécanique, LadHyX-CNRS, École Polytechnique, 91128 Palaiseau, France

ABSTRACT

With an analytical model coupling a mixing layer flow with an oscillating vegetation canopy through a drag force, we show that for both the cases of wind over a wheat field and a water stream over aquatic plants, the dynamics of the plants is responsible for increasing the growth rate of the coupled instability in the lock-in range through two mechanisms. Because the flow and the vegetation canopy move in phase and thus minimise their interactions, the drag dissipation is decreased. The correlation between the two components of the perturbation flow velocity in the mixing layer is increased and make the perturbation flow more efficient at extracting energy from the mean flow.

1. INTRODUCTION

The focus of this paper is the strong coupling between the dynamics of a fluid flow such as the wind or water current and that of a plant canopy. By plant canopy, we mean a large collection of individual plants such as a dense forest, a crop field, or an aquatic plant cover. The perspective we take on the plants is focused on the canopy as a whole; we perceive the canopy as a poroelastic continuum (de Langre, 2008).

Understanding the mechanisms of interactions between flow and a plant canopy is crucial in predicting and avoiding wind-induced damage to forest and crops. Such an understanding is also essential to properly model the heat, mass and momentum exchanges between plants and the atmosphere (Finnigan, 2000) or between aquatic plants and the water stream they thrive in (Ghisalberti and Nepf, 2006).

The structure of the wind over a vegetation canopy is dominated by a Kelvin-Helmholtz (KH) instability due to the difference of air velocity above and inside the canopy (Raupach et al., 1996). A similar phenomenon is observable in aquatic flows over fully-submerged vegetation (Ghisalberti and Nepf, 2002). The KH instability which is due to the presence of an inflection point

in the velocity profile (Ho and Huerre, 1984) engenders coherent eddies of canopy scale which dominate the turbulent motion of the canopy flow. When the vegetation canopy is flexible, these coherent eddies are responsible for wavelike motions at the canopy top. These wavelike motions are called honami on crop fields and monami on aquatic plants.

Py et al. (2006) showed with on-site experiments using an image-correlation technique that honami occurs at the free-vibration frequency of the plants. They also proposed an analytical model which couples a mixing-layer flow with a vegetation canopy free to oscillate. The two-dimensional conservation of momentum equations are coupled to the canopy oscillator equation through a drag term. This linear model predicts a lock-in mechanism similar in form, but different mechanically to what is observed in vortex-induced vibration (de Langre, 2006). By comparing their experimental observations and the theoretical predictions of their model, Py et al. (2006) concluded that “it is thus the lock-in mechanism suggested by the analysis of the coupled model that explains why the coherent wave-motion of the crops occurs at their eigenfrequency independently of [the wind velocity]”.

The aim of the present study is to understand the dynamical interactions between the mixing layer and the vegetation canopy through which the growth rate of the coupled system is increased. To do this, we revisit the linear analytical model developed by Py et al. (2006) which couples the oscillator equation of a stalk of wheat with a perturbed broken line horizontal wind profile through a drag force. We improve slightly the model by not requiring the irrotationality assumption in the flow solution and in order to broaden the applicability of the model, we account for the free surface in the case of submerged aquatic plants.

The article is organised as follows: In Section 2, the model is derived and the energy method is briefly recalled. In Section 3, the stability analysis is performed on two cases: wind on a wheat

field and shallow aquatic flow over submerged vegetation. The study of each case is followed by a comparative dimensionless analysis based on the mass number.

2. COUPLED MODEL

We revisit the linear analytical model developed by Py et al. (2006) which couples a mixing-layer flow with an oscillating vegetation canopy through a drag force. Let us consider the stability of a 2-dimensional inviscid and incompressible flow of fluid of density ρ over a uniform vegetation canopy of height h as depicted in Fig. 1. Its velocity and pressure fields, $V_x(x, y, t)$, $V_y(x, y, t)$ and $P(x, y, t)$, are governed by the Euler equations on which an external body force \vec{f} acts. This body force is caused by every plant in the canopy and therefore depends on the movement of each individual plant. If we assume that the spacing between the plants ℓ is regular and small as compared to the length scale of the perturbations in the flow, we can treat the numerous plants as a continuum. Taking the horizontal displacement of the canopy as $X(x, y, t)$ we can write the body force acting on the fluid inside the canopy as

$$\vec{f} = -\frac{1}{2}\rho\frac{C_D d}{\ell^2}\left|V_x - \frac{\partial X}{\partial t}\right|\left(V_x - \frac{\partial X}{\partial t}\right)\vec{e}_x, \quad (1)$$

where the product $C_D \times d$ is a dimensional drag coefficient assumed to be uniform along the plant height and independent of the flow velocity. It is set to zero outside the canopy ($y > h$). On the flow field, we apply a boundary condition of no penetration at the ground and a different condition at the top of the domain depending on the system: for the wind-wheat system, vanishing vertical velocity at infinite height; and for the aquatic plant system, a free surface at height H .

To model the inflectional mean flow velocity profile, we impose a basic flow $U_b(y)$ which takes the form of a piecewise linear velocity profile defined by a vorticity thickness δ and two velocities: U_1 and U_2 (see Fig. 1).

To model the canopy motions, we use separation of variables $X(x, y, t) = \chi(y)Q(x, t)$ and consider only the fundamental mode of vibration of the plant stem $\chi(y) = y/h$. Upon projection of this mode on the drag force acting on one plant, and upon neglecting both structural and contact damping, we can write the equation governing

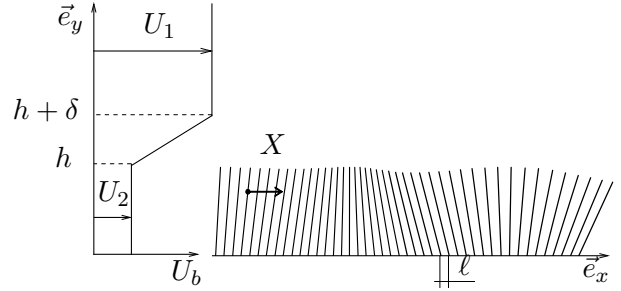


Figure 1: Schematic of the modelled wind profile and crop canopy. Image reproduced from Py et al. (2006).

the dynamics of the canopy as

$$m\frac{\partial^2 Q}{\partial t^2} + m\omega_0^2 Q = -\ell^2 \int_0^h \vec{f} \cdot \vec{e}_x dy, \quad (2)$$

where ω_0 and m are the frequency and the modal mass of the first mode of the plant stem.

To do a dimensionless analysis, we define the mass number, the drag-to-shear ratio, the relative distance of the mixing layer from the ground, the shear parameter, the reduced velocity and the Froude number as

$$M = \frac{m}{\rho h \ell^2}, \quad C = \frac{C_D d \delta}{\ell^2} (1 - R), \quad \bar{h} = \frac{h}{\delta}, \quad (3)$$

$$R = \frac{U_1 - U_2}{U_1 + U_2}, \quad U_R = \frac{U}{\delta \omega_0}, \quad F_R = \sqrt{U^2 / g H},$$

where the scale and timescale are $\bar{t} = tU/\delta$ and $\bar{x} = x/\delta$ and where $U = (U_1 + U_2)/2$ is the average velocity.

We investigate the stability of the basic horizontal velocity \bar{U}_b , to small perturbations of velocity \bar{u} , \bar{v} , pressure \bar{p} , and modal plant deformation \bar{q} . Upon non-dimensionalizing the Euler equations and the oscillator Eq. 2, we can substitute the perturbation scheme and keep only first order quantities to obtain

$$\frac{\partial \bar{u}}{\partial \bar{t}} + \bar{U}_b \frac{\partial \bar{u}}{\partial \bar{x}} + \bar{v} \frac{\partial \bar{U}_b}{\partial \bar{y}} = -\frac{\partial \bar{p}}{\partial \bar{x}} - C \left(\bar{u} - \chi \frac{d\bar{q}}{d\bar{t}} \right) \quad (4)$$

$$\frac{\partial \bar{v}}{\partial \bar{t}} + \bar{U}_b \frac{\partial \bar{v}}{\partial \bar{y}} = -\frac{\partial \bar{p}}{\partial \bar{y}}, \quad (5)$$

$$\frac{\partial \bar{u}}{\partial \bar{x}} + \frac{\partial \bar{v}}{\partial \bar{y}} = 0, \quad (6)$$

$$\frac{\partial^2 \bar{q}}{\partial \bar{t}^2} + U_R^{-2} \bar{q} = \frac{C}{M \bar{h}} \int_0^{\bar{h}} \left(\bar{u} - \chi \frac{\partial \bar{q}}{\partial \bar{t}} \right) \chi d\bar{y}, \quad (7)$$

where we recall that in Eq. 4, C is zero outside the canopy ($\bar{y} > \bar{h}$). We seek a solution to Eqs. 4-7 in the form of a travelling wave $(\bar{u}, \bar{v}, \bar{p}, \bar{q}) = (\hat{u}, \hat{v}, \hat{p}, \hat{q}) e^{i(\bar{k}\bar{x} - \bar{\omega}\bar{t})} + \text{c.c.}$, where \bar{k} and $\bar{\omega}$ are the dimensionless axial wavenumber and complex frequency and where c.c. stands for complex conjugate. For the sake of clarity, the overbars on \bar{k} and $\bar{\omega}$ are omitted from here on.

An analytical general solution to Eqs. 4-6 is found in each y -subdomain corresponding to the three pieces of the mean piecewise velocity profile (see Fig. 1). On these three general flow solutions, we apply seven conditions: the vertical velocity and the pressure must be continuous at the two cuts $\bar{y} = \bar{h}$ and $\bar{y} = \bar{h} + 1$, the solution must respect the travelling-wave form of the boundary conditions, and the oscillator equation 7 must be satisfied. We write these seven conditions on the general solution as a linear operator

$$[\mathbf{L}(U_R, C, M, R, \bar{h}, \omega, k)] \{\vec{A}\} = \{0\}, \quad (8)$$

where \vec{A} represents the 7 integration constants of the general shape functions. We obtain the dispersion relation of the admissible complex frequencies ω with the wavenumbers k by taking the determinant of \mathbf{L} equal to zero. For a given value of k , the corresponding complex values of ω are found with a Müller iterative procedure.

The model described above is essentially that of Py et al. (2006) but differs in three points: we use a different non-dimensionalization, we introduced the free-surface boundary condition, and most importantly we do not assume the flow irrotational. In Py et al. (2006), to simplify the analytical flow solution and obtain a dispersion relation in the form of a polynomial of ω , the flow was assumed irrotational although the canopy drag is clearly dissipative. Because of that assumption, their flow solution did not respect the governing Euler equations. Upon comparing the most unstable complex frequencies predicted with and without the irrotationality assumption, we found that the effect of this assumption on the dynamics of the system is quantitative but not qualitative. For all the results presented here, the irrotationality assumption is not made.

To improve our insight of the flow behaviour, we examine the perturbation flow energy. We apply the energy method described by Drazin and Reid (1981, p. 424) to investigate the energy production and dissipation in the perturbation fluid flow.

The change over time of the perturbation kinetic energy density in the fluid is averaged over

one wavelength $\lambda = 2\pi/k$ and summed over the height of the domain \bar{H} :

$$\frac{\partial E}{\partial t} = \frac{1}{\lambda} \int_0^{\bar{H}} \int_0^\lambda \left(\bar{u} \frac{\partial \bar{u}}{\partial t} + \bar{v} \frac{\partial \bar{v}}{\partial t} \right) d\bar{x} d\bar{y}. \quad (9)$$

The integrand is found by multiplying the linearised equations of motion of the fluid 4-5 by u and v respectively. Upon integration, the divergence terms give a zero global contribution term to the energy balance and we are left with the following non-null terms

$$\frac{\partial E}{\partial t} = P_s - D, \quad (10)$$

where P_s is the energy production from the Reynolds stresses and D is the drag dissipation of the canopy :

$$P_s = -\frac{1}{\lambda} \int_{\bar{h}}^{\bar{h}+1} \int_0^\lambda \bar{u}\bar{v} \frac{\partial \bar{U}_b}{\partial \bar{y}} d\bar{x} d\bar{y}, \quad (11)$$

$$D = \frac{1}{\lambda} \int_0^{\bar{h}} \int_0^\lambda C \left(\bar{u}^2 - \bar{u}\chi \frac{\partial \bar{q}}{\partial \bar{t}} \right) d\bar{x} d\bar{y}. \quad (12)$$

The energy quantities vary in time as $(E, P_s, D) = (\hat{E}, \hat{P}_s, \hat{D}) e^{2\omega_i t}$ and once substituted in Eq. 10, the following identity is immediately derived :

$$\omega_i = \frac{\hat{P}_s}{2\hat{E}} - \frac{\hat{D}}{2\hat{E}}. \quad (13)$$

3. RESULTS

3.1. Wind on a wheat field

The model described in the previous section is used to investigate the instability mechanisms in the interactions between wind and a crop canopy. The parameters kept constant in this analysis are given in Table 1. All values are taken from Py et al. (2006) except the value of R which is taken smaller to amplify the coupling effects; yet it is still in the physically reasonable range considering the very coarse approximation a broken-line profile represents of a real wind profile. As in Py et al., we take $\delta = Rh$.

We study the evolution of the temporal stability of the system with increasing reduced velocity U_R in three configurations: the ‘‘coupled configuration’’ where the Kelvin-Helmholtz (KH) instability in the flow interacts with the flexible plant

	Wheat canopy	Aquatic vegetation
M	0.74	0.0076
C	0.30	0.55
\bar{h}	5	0.36
R	0.2	0.55
\bar{H}_b	∞	15
$F_R U_R^{-1}$	N/A	0.07

Table 1: Dimensionless parameter values used in the simulations.

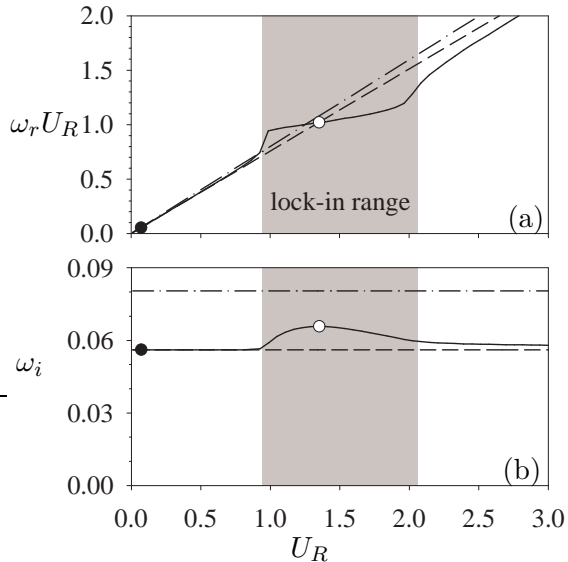


Figure 2: Frequency (a) and growth rate (b) of the wind-wheat system: pure configuration $-\cdot-\cdot-$; heavy configuration $- - -$; coupled configuration $—$. The grey area marks the lock-in range.

canopy, the “pure configuration” where a pure KH instability develops in a flow without vegetation as C is taken vanishingly small, and a “heavy configuration” where a KH instability develops over non-moving vegetation as M is taken very large. For every value of U_R , the most unstable wavenumber of each scenario is considered.

The frequency of the pure configuration shown in dash-dot line in Fig. 2 (a) is known to increase proportionally to the flow velocity (Ho and Huerre, 1984). Its growth rate, shown in Fig. 2 (b), is constant with flow velocity. The frequency of the heavy configuration, in dash line in Fig. 2 (a), is smaller than that of the pure configuration. In the case of the coupled configuration (solid line in Fig. 2), for small and large reduced velocity, the frequency and the growth rate match those of the heavy configuration. This is so because the natural frequency of the plants and that of the KH instability differ greatly hence decoupling their dynamics. For the reduced velocity range corresponding to the grey area in Fig. 2, the fre-

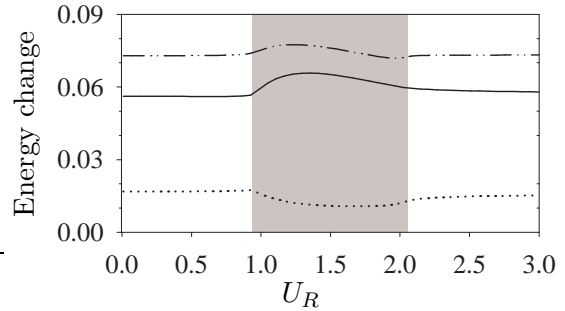


Figure 3: Energy analysis of the wind-wheat system: $\cdot\cdot\cdot\cdot$, $\hat{D}/2\hat{E}$; $-\cdot-\cdot-$, $\hat{P}_s/2\hat{E}$; $—$, ω_i . The grey area marks the lock-in range.

quency of the pure KH instability is closer to the natural frequency of the oscillating wheat stalk and frequency lock-in occurs. As explained by Py et al. (2006), “in this range the frequency of the instability locks onto the frequency of the plants as its value approaches and follows that of the plants.” This leads to an increase in the instability, which can be visualised as a bump in the imaginary frequency plotted in solid line Fig. 2 (b). This imaginary frequency grows larger, yet it remains smaller than that of the pure configuration.

The instability, which is confined to the fluid part of the system at low reduced velocity, spreads to both the fluid and the oscillating canopy in the lock-in range. As a result the dynamics of the plants is responsible for increasing the rate of growth of the instability. This is shown by considering the perturbation energy production and dissipation in the system. The growth rate in solid line, along with the two terms accounting for it in Eq. 13 are plotted in Fig. 3: the production of kinetic energy by the work of the Reynolds stress against the shear ($\hat{P}_s/2\hat{E}$) in dash-dot-dot line and the drag dissipation ($\hat{D}/2\hat{E}$) in dotted line. The Reynolds stresses extract energy from the shear of the basic flow and thus fuel the instability (Drazin and Reid, 1981).

The intensification of the production of perturbation kinetic energy with increasing U_R is caused by more coherence in the mixing layer $\bar{h} < \bar{y} < \bar{h} + 1$. In the lock-in range the correlation between the streamwise and vertical perturbation velocity components increases and has for effect to make the perturbation flow more effective at extracting energy from the mean flow and thus causes the small boost in energy production $\hat{P}_s/2\hat{E}$ as seen in Fig. 3. On the other hand, the decrease of the dissipation $\hat{D}/2\hat{E}$ in Fig. 3 is due

to the fluid inside the canopy and the vegetation moving in phase with one another.

It is understood that as the reduced velocity enters the lock-in range, the most unstable perturbation mode reorganises such that the instability spreads to both the fluid and the oscillating canopy. As the canopy oscillates in phase with the flow, the drag dissipation of kinetic energy is reduced and the work of the Reynolds stresses against the mean flow shear is increased. These two canopy-flow interaction mechanisms contribute to making the system more unstable.

3.2. Shallow aquatic flow over submerged vegetation

Since the same mechanism of coherent vortices produced by the KH instability in the mean flow was identified (Ghisalberti and Nepf, 2002) to be responsible for generating honami and monami, we could think that the effect of the plant dynamics on the flow is similar in both system. As is shown for the wind-wheat system in Subsection 3.1, the dynamics of the aquatic plant canopy is responsible for decreasing the stability of the water flow by diminishing the drag dissipation and boosting the work of the Reynolds stresses in the lock-in velocity range. To show this we use the same approach to investigate the interactions between a shallow water flow and submerged vegetation as in the previous subsection.

The model of Section 2 is applied with the parameter values shown in Table 1 inspired by the model vegetation made of low density polyethylene film of Ghisalberti and Nepf (2002). The added mass and the buoyancy effect are accounted for in the mass number and the reduced velocity. To simplify the analysis and minimise the influence of free-surface waves on the dynamics, the height of the free surface H in our simulations is taken larger than in the experiments of Ghisalberti and Nepf so as to keep the Froude number low. The maximum value of the Froude number reached in the simulations here is $F_R = 0.21$. As in Subsection 3.1 we consider the three configurations: coupled, pure and heavy.

The evolutions with flow velocity of the frequencies and growth rates of the three configurations are plotted in Fig. 4. For very small reduced velocities, the frequency of the coupled configuration follows that of the heavy configuration, but as U_R is increased to a value larger than 0.2, lock-in occurs and the growth rate surges. The lock-in range, identified by the area in grey in Fig. 4, begins at a very small reduced velocity and a frequency only a quarter of the natural

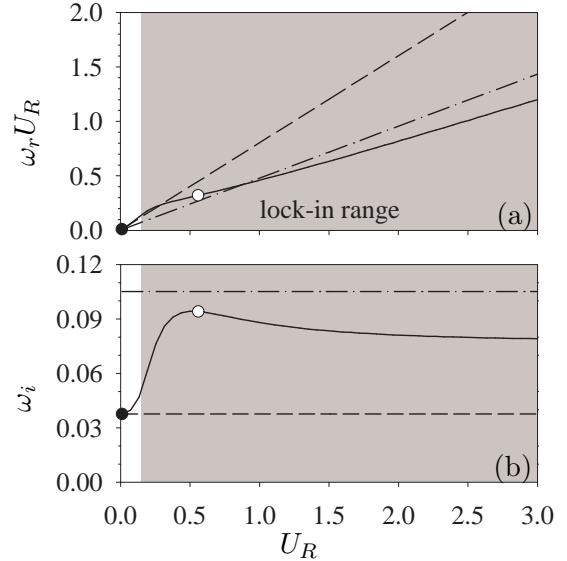


Figure 4: Frequency (a) and growth rate (b) of the aquatic plant system: pure configuration $---$; heavy configuration $- \cdot -$; coupled configuration $---$. The grey area marks the lock-in range.

frequency of the aquatic plants. We still call it “lock-in” even though it does not occur around the natural frequency of the aquatic plants because, as is shown in the following lines, it is still the same mechanisms that are responsible for destabilising further the system.

As in the wind-wheat system, the instability confined to the flow at low reduced velocity spreads to the aquatic plants in the lock-in range and the dynamics of the plants is then responsible for increasing the growth rate of the instability. The increase of ω_i with U_R is plotted in Fig. 5 in solid line along with the two terms of Eq. 13 that accounts for it: $(\hat{P}_s/2\hat{E})$ in dash-dot-dot line and $(\hat{D}/2\hat{E})$ in dotted line. For both the wind-wheat system and the aquatic plant system, two mechanisms are responsible for further destabilising the flow in the lock-in reduced velocity range: a decrease of the drag dissipation; and an increase in the extraction of energy from the mean flow. The lock-in mechanisms are the same in both systems, but from a glance at Figs. 2 and 4, there are obvious differences in the behaviour of both systems. In the next subsection we explain some of these differences with a dimensionless analysis.

3.3. Mass number effect

In the wind-wheat system, the lock-in velocity range is finite and sharp as shown in Fig. 2. The most unstable frequency deviates from that

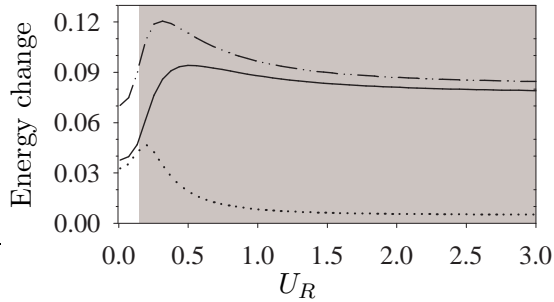


Figure 5: Energy analysis of the aquatic plant system: \cdots , $\dot{D}/2\dot{E}$; $-\cdots-$, $\dot{P}_s/2\dot{E}$; $—$, ω_i . The grey area marks the lock-in range.

of the KH instability to that of the wheat stalk at $U_R = 0.9$ and returns to the KH instability frequency at $U_R = 2.1$. For the aquatic plant system in Fig. 4, past $U_R = 0.2$ the frequency deviates from the KH instability frequency and the growth rate increases abruptly, but the most unstable frequency does not return to the KH instability frequency at higher U_R and the ω_i stays high. The lock-in perpetuates over a very long reduced velocity range. This is due to a low mass number. From Table 1, the wind-wheat system has a mass number, M , almost a hundred times larger than the aquatic plant system (not a thousand times like the fluid density ratio because of the added mass). Decreasing the mass number tends to increase the reduced velocity range over which the lock-in occurs (as noted by Py et al., 2006).

On this mass number effect, a parallel can be drawn with vortex-induced vibrations. The reduced velocity range over which the shedding frequency in the wake of a freely oscillating bluff body locks onto that of the body is significantly increased by diminishing the mass ratio (Williamson and Govardhan, 2004; de Langre, 2006). In vortex-induced vibrations, for small enough mass ratio, lock-in persists up to infinite reduced velocity similarly to what we observe here for the aquatic plant system.

4. CONCLUSION

This model is obviously not meant as a complete simulation of the complex interactions between flow and a plant canopy. Because of its simplicity this model can achieve its goal of singling out the effects due to the coupling of the dynamics of the plants with that of a mixing-layer flow.

For both the wind-wheat system and the aquatic plant system, the instability confined to

the flow at low reduced velocity spreads to the vegetation canopy in the lock-in range. The dynamics of the plants is shown to be responsible for increasing the growth rate of the coupled instability in the lock-in range through two mechanisms: (i) because the flow and the vegetation canopy move in phase and thus minimise their interactions, the drag dissipation is decreased; (ii) the correlation between the two components of the perturbation flow velocity in the mixing layer is increased and make the perturbation flow more efficient at extracting energy from the mean flow.

5. REFERENCES

- de Langre, E., 2006. Frequency lock-in is caused by coupled-mode flutter. *J. Fluids Struct.* 22, 783–791.
- de Langre, E., 2008. Effects of wind on plants. *Annu. Rev. Fluid Mech.* 40, 141–168.
- Drazin, P. G., Reid, W. H., 1981. *Hydrodynamic Stability*. Cambridge University Press.
- Finnigan, J., 2000. Turbulence in plant canopies. *Annu. Rev. Fluid Mech.* 32, 519–571.
- Ghisalberti, M., Nepf, H., 2006. The structure of the shear layers in flows over rigid and flexible canopies. *Environ. Fluid Mech.* 6, 277–301.
- Ghisalberti, M., Nepf, H. M., 2002. Mixing layers and coherent structures in vegetated aquatic flows. *J. Geophys. Res.* 107, 3011.
- Ho, C., Huerre, P., 1984. Perturbed free shear layers. *Annu. Rev. Fluid Mech.* 16, 365–422.
- Py, C., de Langre, E., Moulia, B., 2006. A frequency lock-in mechanism in the interaction between wind and crop canopies. *J. Fluid Mech.* 568, 425–449.
- Raupach, M. R., Finnigan, J. J., Brunet, Y., 1996. Coherent eddies and turbulence in vegetation canopies: The mixing-layer analogy. *Bound.-Lay. Meteorol.* 78, 351–382.
- Tennekes, H., Lumley, J. L., 1972. *A First Course in Turbulence*, MIT Press. Cambridge, Massachusetts.
- Williamson, C. H. K. and Govardhan R., 2004. Vortex-Induced Vibrations. *Annu. Rev. Fluid Mech.* 36, 413–455.